ACS APPLIED MATERIALS & INTERFACES

Research Article

www.acsami.org

Simple Synthesis and Photoelectrochemical Characterizations of Polythiophene/Pd/TiO_2 Composite Microspheres

Yuqiao Wang,*[,†] Wenjing Chu,[†] Shasha Wang,[†] Zehao Li,[†] Yinghao Zeng,[†] Shancheng Yan,*[,‡] and Yueming Sun[†]

[†]Jiangsu Optoelectronic Functional Materials and Engineering Laboratory, School of Chemistry and Chemical Engineering, Southeast University, Nanjing 211189, China

[‡]School of Geography and Biological Information, Nanjing University of Posts and Telecommunications, Nanjing 210023, China

ABSTRACT: We report here a simple, effective, and low cost method to synthesize polythiophene/Pd/TiO_2 (PTh/Pd/TiO_2) ternary composite microspheres and apply such a composite to photoelectrochemical (PEC) sensing. TiO_2 spherical aggregates of 200 nm diameter, consisting of nanoscale building blocks of TiO_2, have been prepared by hydrolysis of tetrabutyl titanate in a water-in-oil emulsion system ($V_{water}/V_{acetone}$ = 1/100). Pd species and PTh layer were decorated onto TiO_2 microspherical substrates by reduction of Pd salts and polymerization of thiophene, respectively. The high surface area, effective charge transfer, and enhanced light absorption of the ternary composite could improve PEC performance under simulated sunlight. The sensitivity, selectivity, and stability of PEC sensor for detecting L-cysteine were much higher than those of the traditional electrochemical sensor. The detection limit of L-cysteine was 9.24 μM in the linear range of 0.31−5.30 mM. Moreover, the results also indicated a good anti-interference and acceptable accuracy in practical application, providing a rapid and sensitive detection method.

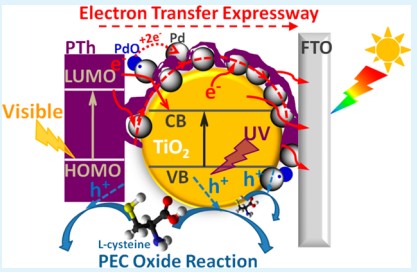

KEYWORDS: *microsphere, composite, photoelectrochemistry, sensor, sensitivity, detection limit*

1. INTRODUCTION

TiO_2 microsphere-based materials have been attracting more and more attention in the promising applications such as energy conversion, environmental remediation, and photoelectrochemical (PEC) detection[1−4] because of their high catalytic activity, long-term stability, and low cost. Their PEC properties are generally determined by the secondary nanoscale building blocks, such as crystal structure and morphology. Template methods have been developed to synthesize TiO_2 microsphere using the template-assisted agents of surfactants,[5,6] ionic liquids,[7,8] and block copolymers.[9,10] However, pure TiO_2 is not an ideal candidate for both visible light absorption and charge transfer because of its large band gap and surface state defect. These weaknesses reduce the use of visible light and increase the recombination rate of photogenerated electrons.

The noble metal/TiO_2 heterogeneous catalysts can be prepared by compositing TiO_2 with noble metals, such as Pd, Ru, Rh, Pt, Au, and Ag, etc., which could promote photocatalytic efficiency, due to strong metal−support interaction (SMSI).[11−13] This effect requires that the TiO_2 supporting matrix has a high specific surface area and the nanoscale noble metal has both outstanding dispersion and stability, which might further improve the synergistic effect of components collaboratively. Among the numerous noble metals, Pd is in great demand because of its unique electronic structure, thermal, and PEC properties. In addition, Pd also could effectively retard the recombination between photogenerated electron and hole (e^-/h^+) pairs at TiO_2 surface.[14,15] However, Pd nanoparticles are usually considered a lack of continuous uniform distribution in view of aggregation, which would decrease electron transfer. Fortunately, coating thin layers of conducting polymers onto Pd/TiO_2 surfaces not only can enhance the conductivity but also can increase the absorption of light. Therefore, the conducting polymer is also a great concern of PEC fields because of its tunable molecular structure and properties, especially in the case of controlling energy level, enhancing light absorption and improving charge transport.[16,17] The typical conducting polymers, such as polythiophene (PTh),[18,19] polypyrrole (PPy),[20,21] polyaniline (PAn),[22,23] and polyindole (PIn),[24,25] with a broad light absorption and efficient charge transport have been employed to decorate semiconductor oxide nanocrystalline (ZnO, TiO_2) for high effective PEC devices.

The PEC detection is a newly developed analytical technique for the sensing platform, which fully integrates the photogenerated carriers and electrochemical signals for detecting the chemical reaction at the photoelectrode surface.[26,27] This coupling effect can make full use of the complete separation between photoirradiation source and current detection signal. Moreover, the undesired background signal could be greatly reduced. Thus, the PEC technique possesses potentially higher sensitivity than the conventional electrochemical and optical methods. Such PEC sensors based on the conducting polymers

Received: August 26, 2014
Accepted: November 7, 2014
Published: November 7, 2014

or quantum dots sensitized photoelectrodes were discussed in the previous literature.[28−31]

Herein, we describe a facile method to synthesize TiO_2 microspheres in water/acetone solvent like a water-in-oil emulsion, where the nanoscale building blocks could be controlled to form uniform spherical aggregates. The microspheres would be loaded by Pd species and then covered with PTh to produce a ternary composite microsphere. Such a composite structure can embody the advantages of each component: (i) TiO_2 microsphere with uniform distribution and high surface area acts as a huge supporting platform; (ii) nanoscale Pd and thin PTh layer offer an electron transfer expressway to separate e^-/h^+ pairs; (iii) PTh layer enhances visible light absorption to increase more photogenerated e^-/h^+ pairs. In addition, PTh was chosen as a coating layer because of its simple and mild synthesis method. To evaluate the promising application of PTh/Pd/TiO_2, we used composite microspheres deposited onto fluorine-doped tin oxide (FTO) as a photoelectrode and assembled a PEC sensor for detecting L-cysteine under simulated sunlight.

2. EXPERIMENTAL SECTION

2.1. Chemicals and Instrumentation. Tetrabutyl titanate (TBTI), thiophene, palladium(II) chloride ($PdCl_2$), and anhydrous ferric chloride ($FeCl_3$) were purchased from Sigma-Aldrich. Sodium dodecylbenzenesulfonate (SDBS), polyvinyl pyrrolidone (PVP), ethylene glycol (EG), and acetone were obtained from Sinopharm Chemical Reagent of China without any further purification. FTO glass (sheet resistance 10 Ω/cm^2) was purchased from Asahi.

The phases were analyzed by X-ray powder diffraction (XRD) using a Philips X'PertPRO with Cu Kα radiation (λ = 1.54 Å). The morphologies were examined by a field-emission scanning electron microscope (FESEM, FEI) and transmission electron microscopy (TEM) and high-resolution TEM (HRTEM) (Tecnai 12) microscopes. Fourier transform infrared (FTIR) spectra were recorded by Bruker Vector. The surface area and pore analysis were assessed by Brunauer−Emmett−Teller (BET) and Barrett−Joyner−Halenda (BJH) procedures (Micromeritics ASAP 2010), respectively. The thermal gravimetric analysis with differential scanning calorimetry (TGA-DSC) was obtained by a SDT Q600, with a heating rate of 20 °C/min in air. Photoluminescence (PL) spectra were measured by F-4600 fluorescence spectrophotometer (Hitachi, Japan) with an excitation wavelength of 350 nm under ambient conditions. X-ray photoelectron spectroscopy (XPS) was performed using Thermo Scientific ESCALAB 250 equipped with Mg Kα radiation ($h\nu$ = 1253.6 eV).

2.2. Preparation of Composite Microspheres. TBTI/EG (2 mL/50 mL) solution was rapidly added to 280 mL of deionized water (DIW)/acetone solvent (V/V = 1/100), and the mixture was kept stirring for 1 h. The colloidal suspension was centrifuged, washed by ethanol, dried at 60 °C in a vacuum, and calcined at 500 °C for 3 h in air. The yield of TiO_2 microsphere could reach 85%. 2.0 mM H_2PdCl_4 solution was prepared by dissolving 0.0887 g of $PdCl_2$ in 6 mL of hydrochloric acid (0.2 M) and further diluting to 250 mL with DIW. Then 15 mL of H_2PdCl_4, 21 mL of DIW, and 0.0333 g of PVP were mixed to form a uniform dispersion system under stirring, and then 14 mL of aqueous alcoholics solution (V/V = 3/2) was added. The mixed solution was refluxed for 3 h to form a Pd colloid solution. TiO_2 microsphere/DIW (0.1277 g/10 mL) suspension was dropped to the Pd colloid solution under stirring for 24 h and then washed by ethanol, dried at 80 °C in a vacuum, and calcined at 350 °C for 2 h in air. The as-prepared Pd/TiO_2 was achieved. Amounts of 0.33 g of Pd/TiO_2 powder, 0.0158 g of SDBS, and 25 μL of thiophene were dispersed in 100 mL of chloroform under ultrasound. An amount of 0.1031 g of $FeCl_3$ was added and stirred for 13 h in an ice−water bath. After reaction, the solvent was removed by the vacuum distillation technique. The crude product was washed with 1.0 M hydrochloric acid to remove the Fe^{3+} ions and washed by DIW to neutral. After drying under vacuum at 60 °C overnight, the yield of PTh/Pd/TiO_2 composite microsphere was 92%.

2.3. Assembly of PEC Sensor. Each of PTh/Pd/TiO_2, Pd/TiO_2, PTh/TiO_2, and TiO_2 was dispersed in ethanol to achieve 10 mg/mL suspending mixtures with ultrasonication. The 15 μL suspensions were cast onto the clean surface of FTO (active area of 0.25 cm^2) and decorated by Nafion and dried to prepare various photoelectrodes. A PEC sensor was assembled with a photoelectrode as a working electrode, Ag/AgCl as a reference electrode, and Pt wire as a counter electrode in 50 mM Na_2SO_4 solution.

All PEC experiments were performed under illumination of CEL-HXE300 xenon lamp with a controlled on/off shut acting as simulated sunlight (wavelength range 300−700 nm, intensity 25 mW/cm^2). Electrochemical impedance spectroscopy (EIS) was carried out by Gamry Reference600 with frequency range of 10^{-1}−10^5 Hz at 5 mV bias voltage. Amperometric response and transient photocurrent were conducted using a CHI760D electrochemical workstation (Shanghai Chenhua Instrument Co., Ltd.). The interference effect on detecting L-cysteine with electroactive species was studied at 0.50 V applied potential.

3. RESULTS AND DISCUSSION

The morphology of TiO_2 microsphere before and after coating with Pd and PTh was observed through TEM. Figure 1a shows

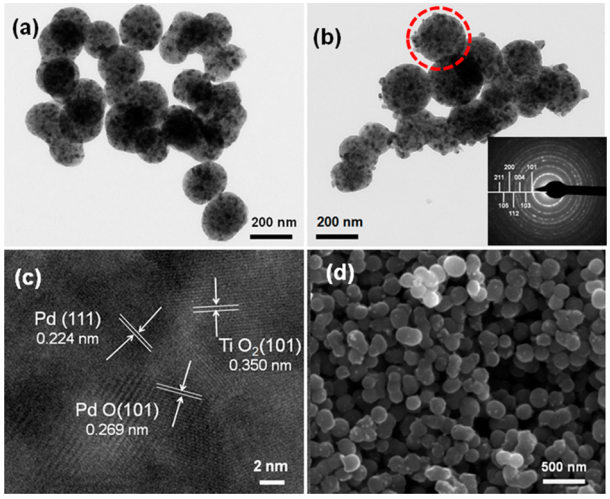

Figure 1. TEM images of (a) pure TiO_2 microsphere and (b) PTh/Pd/TiO_2 composite microsphere, with inset showing a corresponding SAED pattern of the dotted circle part. (c) HRTEM image and (d) SEM image of PTh/Pd/TiO_2 composite microsphere.

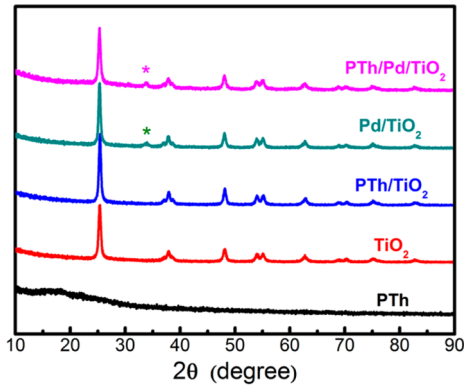

Figure 2. XRD patterns of different components.

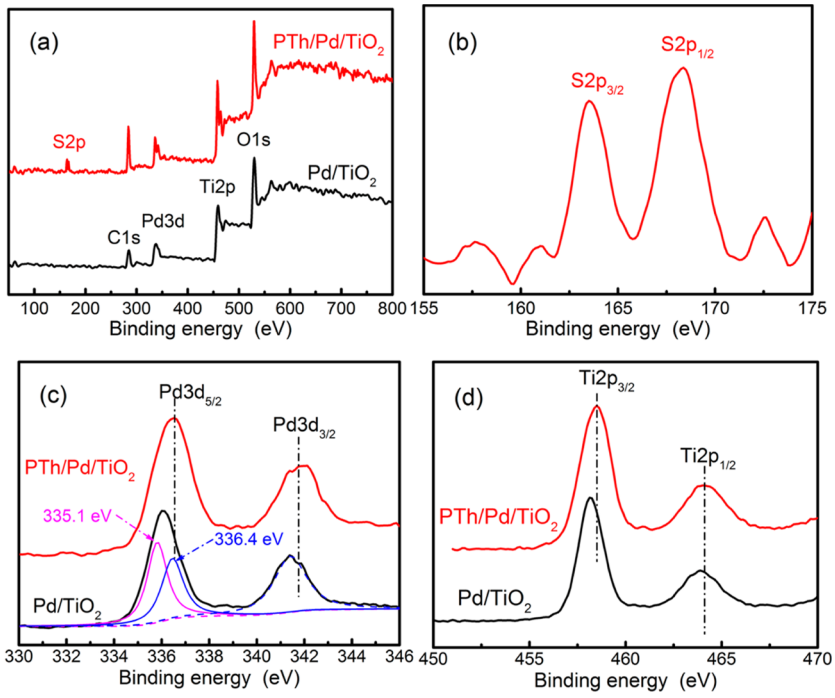

Figure 3. (a) XPS of the composite microspheres of Pd/TiO_2 and $PTh/Pd/TiO_2$. Corresponding high-resolution XPS of (b) S 2p, (c) Pd 3d, and (d) Ti 2p.

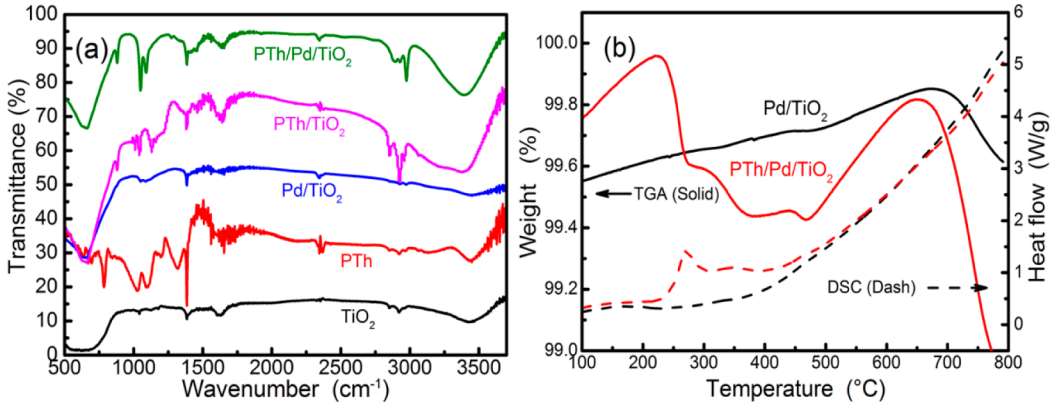

Figure 4. (a) FTIR spectra and (b) TGA-DSC curves of different components.

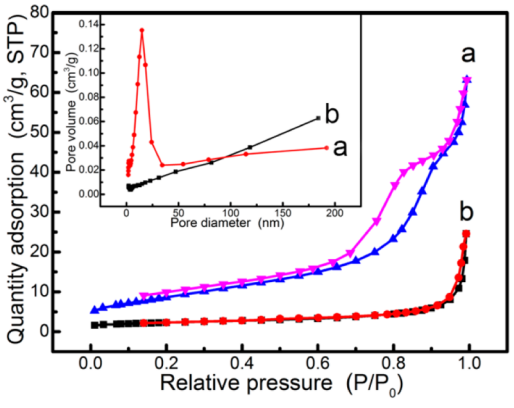

Figure 5. N_2 adsorption−desorption isotherms of (a) $PTH/Pd/TiO_2$ and (b) pure TiO_2 microphere, with an inset showing the corresponding BJH pore size distribution.

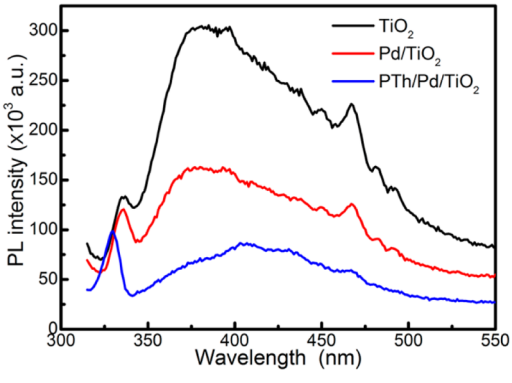

Figure 6. PL spectra of TiO_2 microsphere and Pd/TiO_2 and $PTh/Pd/TiO_2$ composite microsphere. Excitation wavelength is 350 nm.

the bare TiO_2 microspheres with 200 nm diameters. The diameter of $PTh/Pd/TiO_2$ did not obviously increase with PTh/Pd layer growing in Figure 1b. The SAED pattern of

dx.doi.org/10.1021/am505720a | ACS Appl. Mater. Interfaces 2014, 6, 20197−20204

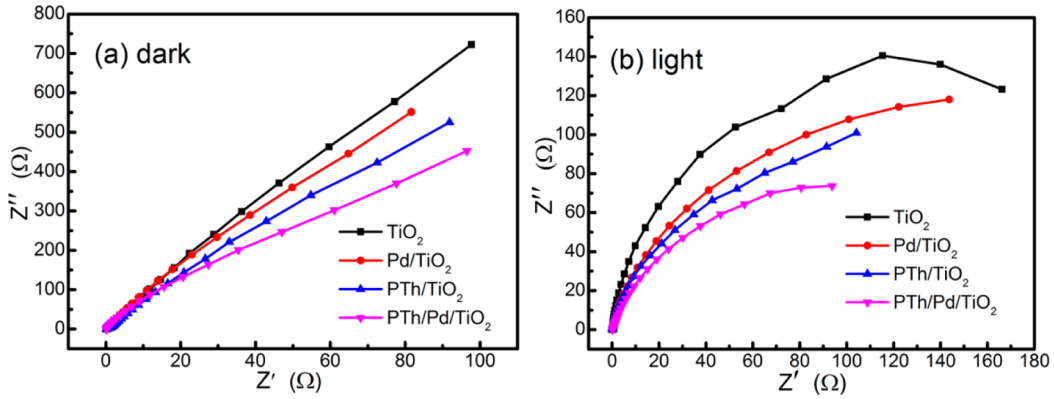

Figure 7. Nyquist plots of EIS based on the TiO_2, Pd/TiO_2, PTh/TiO_2, and $PTh/Pd/TiO_2$ modified FTO acting as photoelectrodes in (a) dark and (b) light (25 mW/cm^2).

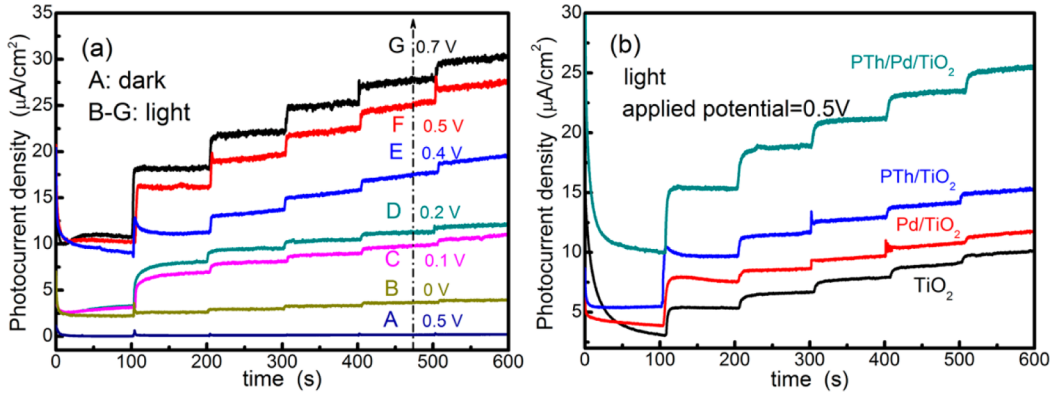

Figure 8. Amperometric responses of the successive addition 0.5 mM L-cysteine on (a) $PTh/Pd/TiO_2$ photoelectrode with different applied potential under illumination except A-curve in the dark and (b) various photoelectrodes under simulated solar illumination (25 mW/cm^2).

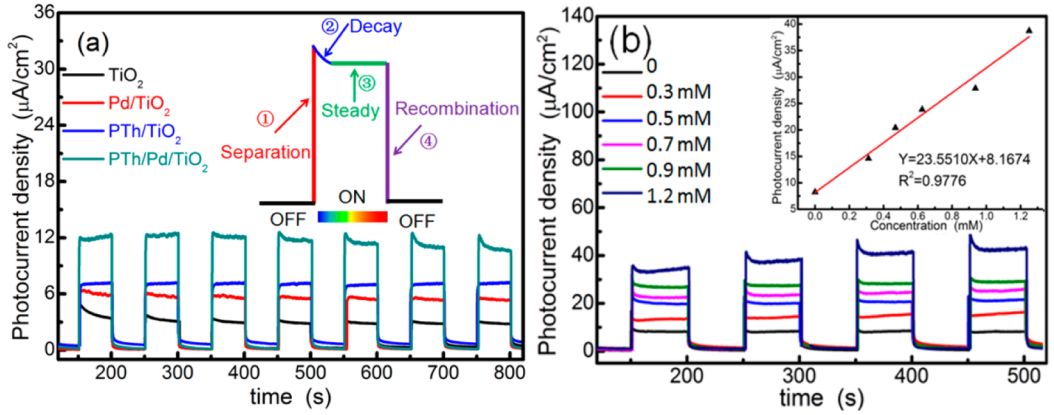

Figure 9. Transient photocurrent response for (a) various materials modified FTO as photoelectrodes with 0.3 mM L-cysteine (inset showing schematic diagram of an ideal photocurrent response), (b) different concentrations (0, 0.3, 0.5, 0.7, 0.9, 1.2 mM) of L-cysteine based on $PTh/Pd/TiO_2$ modified FTO as photoelectrode (inset showing fitting curves of photocurrent intensity vs L-cysteine concentration). Applied potential was 0.5 V vs Ag/AgCl with 50 s simulated solar light (25 mW/cm^2) on/off cycles.

ternary composites indicates the obvious diffraction rings indicative of anatase TiO_2 characteristic peaks, referring to JCPDS no. 21-1272, as shown in the inset of Figure 1b. Compared with the obvious anatase phase, the diffraction rings of Pd species and PTh were not easily observed. As shown in Figure 1c, the HRTEM image of the edge of $PTh/Pd/TiO_2$ displays the lattice spacing of Pd (~0.224 nm), PdO (~0.269 nm), and TiO_2 (~0.350 nm), which agreed well with the (111) crystal planes of Pd, (101) of PdO, and (101) of TiO_2.[32] The results indicated that Pd^0 and Pd^{2+} species might coexist in compounds because of the formation of PdO at high temperature sintering in air. The morphology of $PTh/Pd/TiO_2$ was also observed by SEM image in Figure 1d, implying the uniform dispersion and porous structure, which might seem propitious to catalytic reactions. Nevertheless, the peaks of metallic or oxidized Pd phase could be found from XRD patterns of Figure 2. The very weak peak at 33.9° could be attributed to the PdO (101) reflection (JCPDS no. 41-1107).

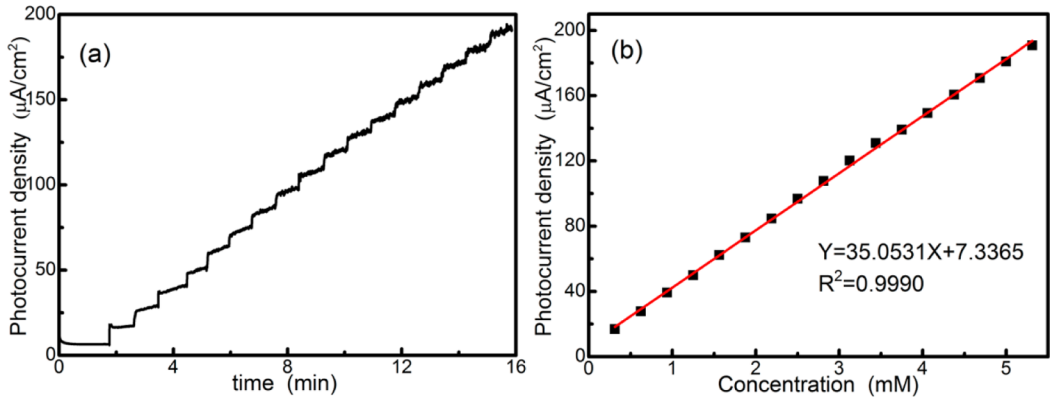

Figure 10. (a) Amperometric response of PTh/Pd/TiO_2 modified FTO as photoelectrode upon successive injection of 0.5 mM L-cysteine. (b) Photocurrent response vs L-cysteine concentration with fitting curve.

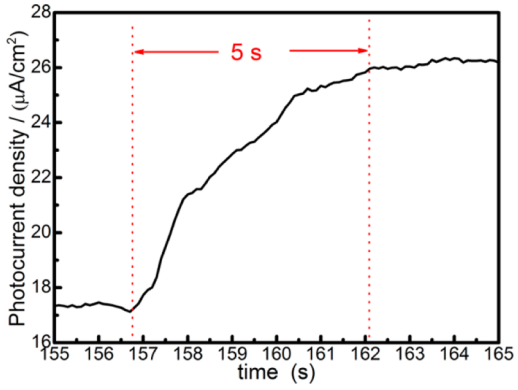

Figure 11. Local amplification step from amperometric response based on PTh/Pd/TiO_2 modified FTO as photoelectrode.

The Pd characteristic peak at 39.9° (JCPDS no. 87-0643) might be obscured by the strong anatase peak at 37.8°. The other peaks of metallic Pd could not be observed for its low content.[21] PTh broad peak was around 18.5° but not observed in composites because of the relative low content. The results revealed that the compound was a ternary composite microsphere with high dispersion and porosity, consisting of metallic and oxidized Pd, anatase TiO_2, and thin layer of amorphous PTh.

To further confirm the surface and electronic state of Pd species and PTh layer, the quantitative XPS analyses of Pd/TiO_2 and PTh/Pd/TiO_2 were performed with their high-resolution spectra. Figure 3a represented two prominent differences, that the S 2p peak appeared around 163−168 eV and XPS intensity of PTh/Pd/TiO_2 was slightly stronger than that of Pd/TiO_2 with area normalization. The results indicated that PTh layer could effectively improve the interaction between Pd species and TiO_2, which might further enhance SMSI effect in PEC process. In high-resolution S 2p of Figure 3b, S $2p_{1/2}$ and S $2p_{3/2}$ positions were consistent with the reported PTh values, suggesting the intactness of the thiophene monomeric unit in the synthesized polymer film.[33] Figure 3c shows Pd $3d_{5/2}$ peak of 336.1 eV and Pd $3d_{3/2}$ peak of 341.3 eV, indicating that the surface-content ratio of Pd species to TiO_2 corresponded to ~0.13 wt % using the peak deconvolution and quantitative analysis.[32] Notably, the peak of 336.1 eV could be decomposed into two peaks at 336.4 and 335.1 eV (Pd/TiO_2 curve), suggesting that the two characteristic peaks were indexed to oxidized and metallic Pd.[34] Considering the PTh layer-covered Pd/TiO_2, the peak of PTh/Pd/TiO_2 shifted to 336.5 eV. Ti $2p_{1/2}$ and Ti $2p_{3/2}$ peaks of Pd/TiO_2 located at 463.9 and 458.1 eV were assigned to the presence of typical Ti^{4+} in TiO_2 microsphere, as shown in Figure 3d. The binding energy difference of 5.8 eV was in good agreement with the reported Pd/TiO_2 sample containing 0.1 mol % Pd.[35] Ti $2p_{3/2}$ peak of PTh/Pd/TiO_2 shifted to 458.8 eV because of the PTh improving interaction between each component, which might contribute to PEC performance.

From the chemisorption point of view, FTIR spectra provided an accurate and direct method to determine the individual PTh and Pd species at TiO_2 surface, as shown in Figure 4a. The broad band around 3450 cm^{-1} was attributed to ν(OH) stretching mode due to the adsorbed water molecules on the sample surface. The narrow bands in the 2975−2850 cm^{-1} range were due to organic residues from the sample preparation procedure. The absorption band at 1650 cm^{-1} in PTh spectrum was from overoxidation of thiophene ring, forming a cetone at β ring positions. The peak at 1510 cm^{-1} corresponded to thiophene ring C=C stretching vibration. The multiple bands were observed at 1200, 1100, 1020, and 787 cm^{-1}, suggesting the formation of PTh backbone chains. The strong and wide bands around 500 cm^{-1} were attributed to metal−O stretching and Ti−O−Ti bridging stretching modes.

Table 1. Comparison of the Sensor Performance Based on Different Methods

method	linear range (mM/L)	sensitivity (μA/(cm² mM))	detection limit (μM)
amperometric reponse[a]	0.05−10.0	22.47	81.20
differential pulse voltammetry[a]	0.1−10.0	21.64	12.80
transient photocurrent response[b]	0.01−1.25	23.55	9.78
amperometric response[b]	0.31−5.31	35.05	9.24

[a]Ref 39. Chemical sensors based on Fe_3O_4/reduced graphene oxide composite-modified glassy carbon electrode. [b]PEC sensors based on PTh/Pd/TiO_2 composite microsphere modified FTO substrate in our current work.

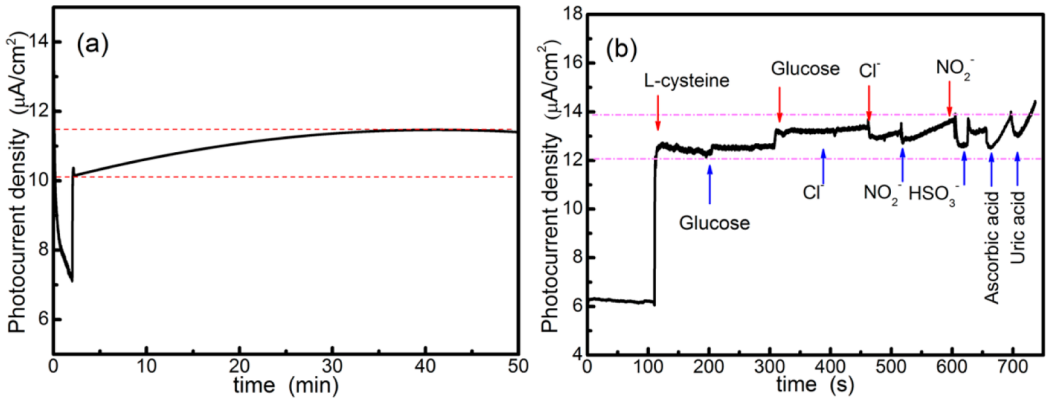

Figure 12. (a) Chronoamperometric stability with 0.6 mM L-cysteine and (b) interference effect of some electroactive ions with 0.6 mM (blue arrow) and 1.3 mM (red arrow) L-cysteine at applied potential of 0.50 V.

In this way, the electron transfer from O to Ti would occur readily, which would promote the SMSI effect.[35,36] This chemical bond bridge interaction was also proved by the O 1s peak of 529.7 eV in Figure 3a, which might originate from metal (Ti^{4+} or Ti^{3+})−O/metal−OH. As a result, FTIR analysis proved the active chemical bonding states of PTh/Pd/TiO_2, which could ensure a high speed channel of electron transfer for PEC reactions. The TGA-DSC technique was used to examine the thermal stability and relative content of samples. For PTh/Pd/TiO_2 in Figure 4b, the exothermic peak appeared at around 269 °C, which might be assigned to the decomposition of PTh. The range of 250−269 °C was the stepwise oxidation process of PTh. The corresponding weight loss of ∼0.8% was caused by PTh decomposition. The next weight loss (<0.1%) gradually started over the temperature range of 269−360 °C, where a tiny amount of PTh with various extremely high molecular weight was decomposed. From 461 to 655 °C, the weight increase became rapid because of the onset of the Pd−PdO transformation. When the temperature exceeded 655 °C, PdO was transformed into Pd.[37] By comparison with PTh/Pd/TiO_2, Pd/TiO_2 weight increase of approximate 0.03% was due to the oxide formation at 655 °C. The result indicated that about 20% Pd was oxidized to PdO. The total content of Pd species was not beyond 0.8%. The results were consistent with data from XRD and XPS, indicating that the content of PTh and Pd was very low. In other words, the PTh/Pd layer was an ultrathin film.

The surface area and porosity are also very important for PEC catalytic reaction. As shown in Figure 5, N_2 adsorption−desorption isotherm measurements indicated a type IV isotherm for mesoporous materials with a typical hysteresis loop. Briefly, N_2 was adsorbed inside PTh/Pd/TiO_2 pores at low pressures, first forming a monolayer, then followed by the multilayer formation, and finally capillary condensation of N_2 occurred during the adsorption process. The hysteresis suggested a mesoporous structure of PTh/Pd/TiO_2 with surface areas of 31.48 m^2/g, average pore diameter of 12.41 nm, and pore volume of 0.098 cm^3/g. Compared with the PTh/Pd/TiO_2 composite microsphere, the hysteresis of pure TiO_2 microsphere was type III isotherm for nanoporous TiO_2, which suggested that pure TiO_2 had slit-shaped pores. The pore size distributions could provide the direct evidence, as shown in the Figure 5 insert. The specific surface area, pore volume, and the average pore size of pure TiO_2 microsphere were 8.11 m^2/g, 18.74 nm, and 0.0085 cm^3/g, respectively. Therefore, PTh/Pd/TiO_2 composite microsphere indicated the mesoporous properties, which could make contributions to the mass transfer during PEC process.

PL emission spectra were employed to monitor the charge transfer efficiency before and after TiO_2 surface modification. Compared with TiO_2 in Figure 6, the PL intensity of the other two samples significantly decreased, indicating that PTh/Pd/TiO_2 had a lower recombination rate of photogenerated electrons than TiO_2 and Pd/TiO_2 samples. The main reason was that both Pd species and PTh layer could help photogenerated electrons to transport to conducting substrates. Therefore, the direct recombination rate of photogenerated e^-/h^+ pairs was retarded, leading to PL signal decrease.[22]

In terms of electrochemistry, the low impedance circuit helps electron transfer, indicating that the corresponding structure is like an electron transfer highway. The result was useful to improve the current signal in some devices. For PEC sensors, this effect would also happen. Nyquist plots are often employed to characterize the charge transfer property of the modified electrode surface, including the charge transfer resistance and the charge separation efficiency. The radius of each arc was correlated with the resistance of electron transfer and separation at the interface between photoelectrode and electrolyte solution. As shown in Figure 7a, the arc radii of various photoelectrodes were like straight lines with 45° angle vs *X*-axis in dark, implying that the impedance was very large or the extremely weak current went through the photoelectrode surface in the absence of light. In contrast to the simulated solar illumination in Figure 7b, the arc radii of Pd/TiO_2 and PTh/TiO_2 were smaller than that of bare TiO_2, indicating that the Schottky junctions formed between Pd or PTh and TiO_2 could facilitate the separation of photoinduced charge carriers and interfacial transfer of electrons.[15,38] The arc radius of PTh/Pd/TiO_2 was the smallest of the four samples based on the ternary synergistic effect, suggesting that the lowest charge transfer resistance was good at enhancing the interfacial interaction, promoting the efficiency of charge transport and accelerating the separation of photogenerated e^-/h^+ pairs.

To further estimate PEC catalytic ability of PTh/Pd/TiO_2 photoelectrode, the amperometric response was used to detect L-cysteine under the different applied potentials in Figure 8a. With increasing applied potential, the step height of current response became larger. The obvious amperometric step appeared at 0.50 V under illumination (F curve), while the signal was much smaller when light was off (A curve). When the voltage rose to 0.7 V, the increase of current amplitude was not obvious. Considering technique and cost, the applied

voltage of 0.5 V was used in the next experiment. The results suggested that the light stimulation could enhance the catalytic activity of photoelectrode surface due to the visible light absorption of PTh. For different photoelectrodes in Figure 8b, the largest current response occurred in the PTh/Pd/TiO_2 photoelectrode, suggesting that the ternary composite-modified electrode could act as a PEC sensor working electrode.

Transient photocurrent response is often used to detect the process of charge transfer and separation through the periodic on/off cycles of irradiation, which can be explained by the schematic representation, as shown in the inset of Figure 9a. The initial photocurrent spike is caused by separating photogenerated e^-/h^+ pairs between the photosensitive substance and the semiconductor surface. Subsequently, the photoinduced electrons are injected into the conducting band of semiconductor and then transported to the back contact. Simultaneously, the holes are moved toward the photosensitive substance and then trapped or reduced by the species in the electrolyte. As soon as the electron yield rate and the recombination rate achieve a state of equilibrium, the steady state photocurrent density is achieved. Once the irradiation is switched off, the separated e^-/h^+ pairs immediately recombine. Briefly, the repeated on/off cycles consist of four processes: fast separation, slow decay, steady state, and fast recombination. It is worth noting that the strongest response of separation in the first cycle indicated the fresh photoelectrode activation in the initial application. Obviously, the transient photocurrent response of PTh/Pd/TiO_2 photoelectrode was stronger than that of other electrodes. At least this result can support the following major concerns: (i) TiO_2 microsphere is a good e^-/h^+ separation shunt; (ii) Pd or PTh decorated TiO_2 can enhance photocurrent response, respectively; (iii) PTh/Pd coating TiO_2 can more greatly improve the photocurrent. Under optimized conditions in Figure 9b, the well-defined typical transient photocurrent response for L-cysteine detection at PTh/Pd/TiO_2 photoelectrode was obtained with a good linear range of 0.01−1.25 mM and a high sensitivity of 23.55 $\mu A/(cm^2\ mM)$. The detection limit was estimated to be 9.78 μM by the photocurrent density vs concentration calibration curve (signal-to-noise ratio of 3, $S/N = 3$), as shown in the inset of Figure 9b, which was lower than 12.80 μM of electrochemical biosensor using Fe_3O_4/reduced graphene oxide nanocomposite.[39]

Since amperometry is considered as a reliable detecting method for its sensitivity and stability, this technique was also employed to estimate the detection limit of PEC sensor. As shown in Figure 10a, the representative amperometric response was examined by successively increasing the concentration of L-cysteine under optimized conditions. The calibration curve ($S/N = 3$) of photocurrent density vs concentration was fitted by the regression equations to calculate the detection limit of 9.24 μM with a linear range from 0.31 to 5.31 mM and a high sensitivity of 35.05 $\mu A/(cm^2\ mM)$, which was in accord with results of transient photocurrent response vs concentration curve in Figure 10b. The maximum steady-state current could be achieved about 5 s in Figure 11, indicating a rapid diffusion process of L-cysteine in the mesoporous PTh/Pd/TiO_2 photoelectrode. The main performances of the similar sensor based on the traditional electrochemical detection and PEC detection were collected in Table 1. Obviously, PEC sensor is better than others.

The chronoamperometric response was carried out on 0.5 mM L-cysteine to observe the sensor stability within 30 min as an excellent linear change in Figure 12a. Thereafter, the current was kept under constant response. The result confirmed that PEC sensor based on PTh/Pd/TiO_2 photoelectrode had enough stability testing time to act as a practical device. To assess the selectivity of PEC sensor, the interference of some possible electroactive chemicals was examined in real sample determinations, such as glucose, Cl^-, NO_2^-, HSO_3^-, ascorbic acid, and uric acid. After the different volumes of interfering analytes were injected into the monitoring system, the current variance was smaller than 5% in Figure 12b, where the photocurrent change was still kept in the dotted line range. The result implied that the excellent selectivity of PEC sensor might contribute to PEC oxidation process of L-cysteine in the real test. Certainly, we acknowledge that the practical application of PEC sensor should be estimated by the real sample detection.

4. CONCLUSIONS

We synthesized PTh/Pd/TiO_2 composite microsphere and used it in a PEC sensor for detecting L-cysteine. This ternary compound integrates the advantages of each component, including high surface area, effective charge transfer, and enhanced light absorption. Considering these advantages, the PEC sensor exhibits a high upper detection limit, acceptable accuracy, excellent selectivity, and anti-interference. We believe that this novel insight could be developed in the integration of photogenerated process with electrochemistry, which could be used in the detection of biomolecules.

AUTHOR INFORMATION

Corresponding Authors

*Y.W.: phone, +86 25 52090619; fax, +86 25 52090621; e-mail, yqwang@seu.edu.cn.

*S.Y.: e-mail, yansc@njupt.edu.cn.

Notes

The authors declare no competing financial interest.

ACKNOWLEDGMENTS

This work was financially supported by the National Natural Science Foundation of China (Grants 21173042, 61205057), National Basic Research Program of China (973 Program) (Grant 2013CB932902), Natural Science Foundation of Jiangsu (Grant BK20141338), Science & Technology Support Project of Jiangsu (Grant BE2013118), and Special Funds for Transformation of Scientific & Technological Achievements of Jiangsu (Grant BA2014069).

REFERENCES

(1) Liu, B.; Liu, L. M.; Lang, X. F.; Wang, H. Y.; Lou, X. W.; Aydil, E. S. Doping High-Surface-Area Mesoporous TiO_2 Microspheres with Carbonate for Visible Light Hydrogen Production. *Energy Environ. Sci.* **2014**, *7*, 2592−2597.

(2) Fabregat, G.; Estrany, F.; Casas, M. T.; Aleman, C.; Armelin, E. Detection of Dopamine Using Chemically Synthesized Multilayered Hollow Microspheres. *J. Phys. Chem. B* **2014**, *118*, 4702−4709.

(3) Gao, P.; Liu, Z.; Tai, M.; Sun, D. D.; Ng, W. Multifunctional Graphene Oxide−TiO_2 Microsphere Hierarchical Membrane for Clean Water Production. *Appl. Catal., B* **2013**, *138*, 17−25.

(4) Ma, Y.; Ji, G.; Ding, B.; Lee, J. Y. Facile Solvothermal Synthesis of Anatase TiO_2 Microspheres with Adjustable Mesoporosity for the Reversible Storage of Lithium Ions. *J. Mater. Chem.* **2012**, *22*, 24380−24385.

(5) Liu, S.; Yu, J.; Jaroniec, M. Tunable Photocatalytic Selectivity of Hollow TiO_2 Microspheres Composed of Anatase Polyhedra with Exposed {001} Facets. *J. Am. Chem. Soc.* **2010**, *132*, 11914−11916.

(6) Zheng, Z.; Huang, B.; Qin, X.; Zhang, X.; Dai, Y.; Jiang, M.; Wang, P.; Whangbo, M. H. Highly Efficient Photocatalyst: TiO_2 Microspheres Produced from TiO_2 Nanosheets with a High Percentage of Reactive {001} Facets. *Chem.—Eur. J.* **2009**, *15*, 12576−12579.
(7) Ma, Z.; Yu, J.; Dai, S. Preparation of Inorganic Materials Using Ionic Liquids. *Adv. Mater.* **2010**, *22*, 261−285.
(8) Yu, S.; Liu, B.; Wang, Q.; Gao, Y.; Shi, Y.; Feng, X.; An, X.; Liu, L.; Zhang, J. Ionic Liquid Assisted Chemical Strategy to TiO_2 Hollow Nanocube Assemblies with Surface-Fluorination and Nitridation and High Energy Crystal Facet Exposure for Enhanced Photocatalysis. *ACS Appl. Mater. Interfaces* **2014**, *6*, 10283−10295.
(9) Zhou, W.; Li, W.; Wang, J. Q.; Qu, Y.; Yang, Y.; Xie, Y.; Zhang, K.; Wang, L.; Fu, H.; Zhao, D. Ordered Mesoporous Black TiO_2 as Highly Efficient Hydrogen Evolution Photocatalyst. *J. Am. Chem. Soc.* **2014**, *136*, 9280−9283.
(10) Wu, L.; Sun, W.; Chen, M.; Zhou, S. Synthesis of Hierarchically Nanostructured TiO_2 Spheres with Tunable Morphologies Based on a Novel Amphiphilic Polymer Precursor and Their Use for Heavy Metal Ion Sequestration. *J. Mater. Chem. A* **2014**, *2*, 14004−14013.
(11) Tauster, S. J. Strong Metal−Support Interactions. *Acc. Chem. Res.* **1987**, *20*, 389−394.
(12) Zhang, S. T.; Li, C. M.; Yan, H.; Wei, M.; Evans, D. G.; Duan, X. Density Functional Theory Study on the Metal−Support Interaction between Ru Cluster and Anatase TiO_2(101) Surface. *J. Phys. Chem. C* **2014**, *118*, 3514−3522.
(13) Weerachawanasak, P.; Mekasuwandumrong, O.; Arai, M.; Fujita, S. I.; Praserthdam, P.; Panpranot, J. Effect of Strong Metal−Support Interaction on the Catalytic Performance of Pd/TiO_2 in the Liquid-Phase Semihydrogenation of Phenylacetylene. *J. Catal.* **2009**, *262*, 199−205.
(14) Guo, K.; Li, M.; Fang, X.; Liu, X.; Sebo, B.; Zhu, Y.; Hu, Z.; Zhao, X. Preparation and Enhanced Properties of Dye-Sensitized Solar Cells by Surface Plasmon Resonance of Ag Nanoparticles in Nanocomposite Photoanode. *J. Power Sources* **2013**, *230*, 155−160.
(15) Zhang, Z.; Yu, Y.; Wang, P. Hierarchical Top-Porous/Bottom-Tubular TiO_2 Nanostructures Decorated with Pd Nanoparticles for Efficient Photoelectrocatalytic Decomposition of Synergistic Pollutants. *ACS Appl. Mater. Interfaces* **2012**, *4*, 990−996.
(16) Luo, X.; Weaver, C. L.; Tan, S.; Cui, X. T. Pure Graphene Oxide Doped Conducting Polymer Nanocomposite for Bio-Interfacing. *J. Mater. Chem. B* **2013**, *1*, 1340−1348.
(17) Gangopadhyay, R.; De, A. Conducting Polymer Nanocomposites: A Brief Overview. *Chem. Mater.* **2000**, *12*, 608−622.
(18) Han, Z.; Zhang, J.; Yang, X.; Zhu, H.; Cao, W. Synthesis and Photoelectric Property of Poly (3-Methoxythiophene)/Titanium Dioxide Complexes. *Sol. Energy Mater. Sol. Cells* **2010**, *94*, 755−760.
(19) Lin, J. F.; Tu, G. Y.; Ho, C. C.; Chang, C. Y.; Yen, W. C.; Hsu, S. H.; Chen, Y. F.; Su, W. F. Molecular Structure Effect of Pyridine-Based Surface Ligand on the Performance of P3HT:TiO_2 Hybrid Solar Cell. *ACS Appl. Mater. Interfaces* **2013**, *5*, 1009−1016.
(20) Fan, Q.; Lei, L.; Yin, G.; Sun, Y. Self-weaving CNT-$LiNbO_3$ Nanoplate-Polypyrrole Hybrid as a Flexible Anode for Li-Ion Batteries. *Chem. Commun.* **2014**, *18*, 2370−1373.
(21) Yang, Y.; Wen, J.; Wei, J.; Xiong, R.; Shi, J.; Pan, C. Polypyrrole-Decorated Ag-TiO_2 Nanofibers Exhibiting Enhanced Photocatalytic Activity under Visible-Light Illumination. *ACS Appl. Mater. Interfaces* **2013**, *5*, 6201−6207.
(22) Ansari, M. O.; Khan, M. M.; Ansari, S. A.; Raju, K.; Lee, J.; Cho, M. H. Enhanced Thermal Stability under DC Electrical Conductivity Retention and Visible Light Activity of Ag/TiO_2@Polyaniline Nanocomposite Film. *ACS Appl. Mater. Interfaces* **2014**, *6*, 8124−8133.
(23) Pei, Z.; Ding, L.; Lu, M.; Fan, Z.; Weng, S.; Hu, J.; Liu, P. Synergistic Effect in Polyaniline-Hybrid Defective ZnO with Enhanced Photocatalytic Activity and Stability. *J. Phys. Chem. C* **2014**, *118*, 9570−9577.
(24) Unal, H. I.; Sahan, B.; Erol, O. Effect of Surfactant on Electrokinetic Properties of Polyindole/TiO_2-Conducting Nanocomposites in Aqueous and Nonaqueous Media. *Colloid Polym. Sci.* **2013**, *292*, 499−509.
(25) Döşlü, S. T.; Mert, B. D.; Yazıcı, B. Polyindole Top Coat on TiO_2 Sol−Gel Films for Corrosion Protection of Steel. *Corros. Sci.* **2013**, *66*, 51−58.
(26) Wang, P.; Dai, W.; Ge, L.; Yan, M.; Ge, S.; Yu, J. Visible Light Photoelectrochemical Sensor Based on Au Nanoparticles and Molecularly Imprinted Poly(*o*-phenylenediamine)-Modified TiO_2 Nanotubes for Specific and Sensitive Detection Chlorpyrifos. *Analyst* **2013**, *138*, 939−945.
(27) Wang, G.; Xu, J.; Chen, H. Progress in the Studies of Photoelectrochemical Sensors. *Sci. China, Ser. B* **2009**, *52*, 1789−1800.
(28) Shi, H.; Zhao, G.; Liu, M.; Zhu, Z. A Novel Photoelectrochemical Sensor Based on Molecularly Imprinted Polymer Modified TiO_2 Nanotubes and Its Highly Selective Detection of 2,4-Dichlorophenoxyacetic Acid. *Electrochem. Commun.* **2011**, *13*, 1404−1407.
(29) Lu, B.; Liu, M.; Shi, H.; Huang, X.; Zhao, G. A Novel Photoelectrochemical Sensor for Bisphenol A with High Sensitivity and Selectivity Based on Surface Molecularly Imprinted Polypyrrole Modified TiO_2 Nanotubes. *Electroanalysis* **2013**, *25*, 771−779.
(30) Wang, W.; Bao, L.; Lei, J.; Tu, W.; Ju, H. Visible Light Induced Photoelectrochemical Biosensing Based on Oxygen-Sensitive Quantum Dots. *Anal. Chim. Acta* **2012**, *744*, 33−38.
(31) Yue, Z.; Lisdat, F.; Parak, W. J.; Hickey, S. G.; Tu, L.; Sabir, N.; Dorfs, D.; Bigall, N. C. Quantum-Dot-Based Photoelectrochemical Sensors for Chemical and Biological Detection. *ACS Appl. Mater. Interfaces* **2013**, *5*, 2800−2814.
(32) Ortel, E.; Sokolov, S.; Zielke, C.; Lauermann, I.; Selve, S.; Weh, K.; Paul, B.; Polte, J.; Kraehnert, R. Supported Mesoporous and Hierarchical Porous Pd/TiO_2 Catalytic Coatings with Controlled Particle Size and Pore Structure. *Chem. Mater.* **2012**, *24*, 3828−3838.
(33) Natarajan, S.; Kim, S. H. Synthesis-in-Place of Highly-Conjugated Oligothiophene Micropatterns via Photo-Activated Ullmann Coupling on Copper Surface. *Chem. Commun.* **2006**, *7*, 729−731.
(34) Zhang, C.; Li, Y.; Wang, Y.; He, H. Sodium-Promoted Pd/TiO_2 for Catalytic Oxidation of Formaldehyde at Ambient Temperature. *Environ. Sci. Technol.* **2014**, *48*, 5816−5822.
(35) Kwak, B. S.; Chae, J.; Kim, J.; Kang, M. Enhanced Hydrogen Production from Methanol/Water Photo-Splitting in TiO_2 Including Pd Component. *Bull. Korean Chem. Soc.* **2009**, *30*, 1047−1053.
(36) Panpranot, J.; Kontapakdee, K.; Praserthdam, P. Effect of TiO_2 Crystalline Phase Composition on the Physicochemical and Catalytic Properties of Pd/TiO_2 in Selective Acetylene Hydrogenation. *J. Phys. Chem. B* **2006**, *110*, 8019−8024.
(37) Datye, A. K.; Bravo, J.; Nelson, T. R.; Atanasova, P.; Lyubovsky, M.; Pfefferle, L. Catalyst Microstructure and Methane Oxidation Reactivity during the Pd↔PdO Transformation on Alumina Supports. *Appl. Catal., A* **2000**, *198*, 179−196.
(38) Albery, W. J.; O'Shea, G. J.; Smith, A. L. Interpretation and Use of Mott−Schottky Plots at the Semiconductor/Electrolyte Interface. *J. Chem. Soc. Faraday Trans.* **1996**, *92*, 4083−4085.
(39) Wang, Y.; Liu, Q.; Qi, Q.; Ding, J.; Gao, X.; Zhang, Y.; Sun, Y. Electrocatalytic Oxidation and Detection of *N*-Acetylcysteine Based on Magnetite/Reduced Graphene Oxide Composite-Modified Glassy Carbon Electrode. *Electrochim. Acta* **2013**, *111*, 31−40.